Batteries & Supercaps

Research Article
doi.org/10.1002/batt.202300389

Chemistry Europe
European Chemical Societies Publishing

www.batteries-supercaps.org

Construction of a Magnetic Interphase for Stable Cycling of Lithium Metal Batteries

Yunyi Chen,[a, b] Haijian Liu,[a, b] Lingli Liu,[c] Jiayan Li,[a] and Yongsheng Han*[a, b]

Lithium (Li) metal has been considered to be the most promising anode material. However, the uncontrolled growth of Li dendrites and the instability of the solid electrolyte interphase (SEI) plague the commercial application of Li anodes. In this paper, a dual-functional artificial magnetic interphase composed of PVDF and γ-Fe_2O_3 is designed and constructed on the anode surface. The magnetic interphase modulates the distribution of lithium ions near the interface to induce stable deposition and stripping processes. Meanwhile, the magnetic particles improve the mechanical properties of the SEI layer and suppress the growth and spread of Li dendrites. The symmetrical cell coated with the magnetic layer has a stable cycle life of more than 4000 hours which is longer than that reported in most literature under the same conditions. This study highlights the significance of the magnetic field in stabilizing lithium metal anodes, providing new insights and approaches to develop efficient batteries by matching the diffusion and reaction processes in batteries.

Introduction

With the popularity of cutting-edge consumer electronics, lithium secondary batteries have been widely used as energy storage components for mobile terminals.[1] Meanwhile, the application scope of lithium secondary batteries has further expanded to fields such as electric vehicles, aerospace, and smart grids.[2] It is estimated that the global battery market currently exceeds $100 billion and is expected to reach $135.43 billion by 2027.[1b] This also puts forward higher requirements for lithium batteries in terms of energy density, power density, service life, and safety. The theoretical specific capacity of graphite anode used in traditional lithium-ion batteries is only 372 mAh g^{-1}, and it is urgent to replace the battery anode materials. Lithium metal is considered the "holy grail" of anode materials because of its ultra-high theoretical specific capacity (3860 mAh g^{-1}) and low reduction potential (−3.04 V vs. standard hydrogen electrode).[3] Substituting the current graphite anode with lithium metal has broad prospects for increasing the energy density of lithium batteries. However, in the rapid charge/discharge of lithium metal anode materials, the reaction rate of electrode surface is much faster than the ion mass transfer rate, resulting in the formation of a concentration gradient at the interface. This makes lithium ions easy to gather in a certain place deposition and stripping, resulting in the growth of lithium dendrites and the generation of pits, and resulting in lithium powder and the generation of dead lithium, bringing great security risks. Therefore, under high power density operation (high current density), the safety and stability of lithium anode need to be improved. It is found that the reason for the inhomogeneous deposition caused by limited interfacial mass transfer is the low conductivity of lithium ion in the solid electrolyte interphase (SEI).[4]

The solid electrolyte interphase (SEI) spontaneously formed on the surface of the lithium anode plays a pivotal role in the deposition/stripping process of lithium, which is directly related to the occurrence of the series mentioned above problems and affects the electrochemical performance of the battery. It is a thin layer formed on the surface of the lithium anode due to the side reaction of the electrolyte during the charge and discharge process.[5] The ideal SEI layer has high ionic conductivity and low electronic conductivity. It acts as a "parclose" to inhibit the further breakdown of the electrolyte.[6] However, in batteries with traditional electrolyte systems, the native SEI film on the surface of lithium metal is chemically heterogeneous and structurally unstable, and the diffusion rate of lithium ions is low, resulting in the formation of a concentration gradient at the interface, which promotes the uneven deposition/stripping of lithium, resulting in dramatic changes in the surface volume and morphology of the lithium anode.[7]

Recent advances have shown promise for improving Li deposition/stripping by optimizing SEI layer composition, but these strategies are often incomplete. Such as using additives in the electrolyte to stabilize the SEI,[8] applying high or locally high-concentration electrolytes to optimize the SEI composition,[9] or the employment of electrolytes containing fluorinated solvents.[10] Considering its fast Li-ion diffusion pathway, inorganic-rich SEIs are considered to be ideal for enhancing the interfacial stability of Li metal anodes. Unfortu-

[a] Dr. Y. Chen, H. Liu, J. Li, Prof. Y. Han
State Key Laboratory of Multiphase Complex Systems
Institute of Process Engineering
Chinese Academy of Sciences
Beijing 100190 (China)
E-mail: yshan@ipe.ac.cn

[b] Dr. Y. Chen, H. Liu, Prof. Y. Han
School of Chemical Engineering, University of Chinese Academy of Sciences
Beijing 100049 (China)

[c] Dr. L. Liu
School of Energy, Materials and Chemical Engineering
Hefei University
Hefei 230601 (China)

Supporting information for this article is available on the WWW under https://doi.org/10.1002/batt.202300389

Research Article
doi.org/10.1002/batt.202300389
Chemistry Europe
European Chemical Societies Publishing

nately, these methods usually only work at relatively low current densities. This type of SEI is also prone to rupture when huge volume changes occur during repeated plating/stripping of Li metal, which leads to the failure of the protection of the Li metal anode during long-term cycling. The fracture site has become a "hot spot" conducive to the local enrichment of lithium ions, thus promoting the nucleation and growth of dendrites. Immediately afterward, researchers began to try to construct an artificial SEI layer on the electrode surface to regulate the distribution of lithium ions, and have shown promising results.[11] But many of these attempts have struggled to balance the two key properties of artificial protective layers, mechanical strength and ionic conductivity.[12] Therefore, constructing dual-functional SEI layers to address large volume changes during dynamic Li deposition and stripping remains a major challenge.

Here, we stabilized the lithium plating and stripping behavior by coating a bifunctional artificial magnetic SEI layer composed of PVDF and γ-Fe_2O_3 on the electrode surface. Among them, PVDF endows the coating with the characteristics of stretching and forming feasibility, and the introduction of γ-Fe_2O_3 can not only generate a magnetic field weakening concentration gradient on the electrode surface, but also optimize the conduction mode of lithium ions in PVDF to match the reaction-diffusion behavior of the interface. At the same time, the rigid magnetic particles can enhance the mechanical properties of the protective layer, making Young's modulus as high as 8.22 GPa. Through this strategy, the Li metal anode coated with an artificial magnetic SEI film shows excellent interface stability and achieves ultra-long stable cycling of lithium symmetrical cells exceeding 4000 h. We believe that the design of the magnetic layer can not only be used to improve the stability of Li metal anodes, but also be extended to other artificial SEI designs for various electrode materials.

Results and Discussion

In conventional electrolyte systems, lithium metal can spontaneously react with organic electrolytes to form brittle, heterogeneous, and low ionic conductivity solid electrolyte interphase (SEI). During the rapid lithium plating process, due to the slow transport rate of lithium ions in the SEI layer, it is liable to form a concentration gradient at the interface and induce dendrite growth, as shown in Figure 1(a). The native SEI is vulnerable to dendrite growth and electrode volume changes. Subsequently, the fresh lithium is then exposed to and reacts with the electrolyte. As a result, new SEIs are constantly being created. During Li stripping, dendritic lithium is easily broken off from the roots and becomes isolated lithium. The continuously generated SEI and dead lithium form a thick surface layer on the Li anode, which leads to a continuous increase in interfacial resistance, exacerbates the uneven Li deposition/stripping, and forms a vicious circle. Therefore, in order to match the reaction and diffusion at the interface of the Li metal anode, it is particularly important to construct an SEI layer that integrates fast ion transport channels and strong mechanical properties. Ex-situ coatings consist of polymers (such as PVDF), inorganic ceramics, and their hybrid materials, which can provide strong mechanical strength, thereby essentially overcoming the fragility problem of in-situ SEI. However, low ionic conductivity, insufficient mechanical robustness of polymers, and poor interfacial contact of ceramics remain great challenges for the fabrication of efficient dendrite-free Li metal anodes (Figure 1b).

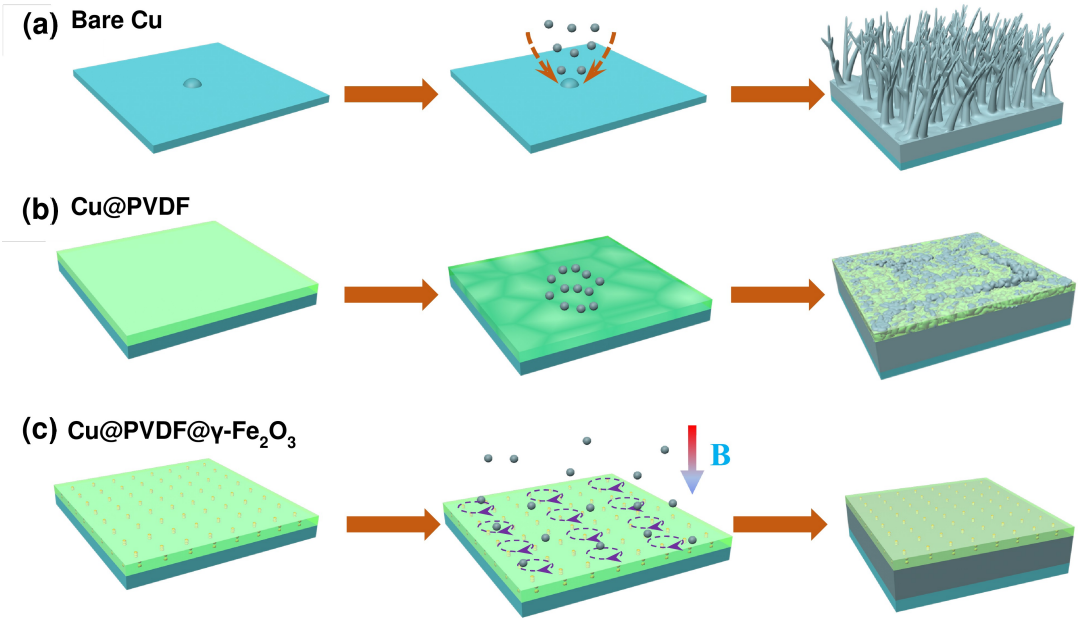

Figure 1. Schematic illustrations of Li deposition morphologies. a) Without artificial protective SEI, inhomogeneous lithium deposition causes dendrite growth after charge-discharge cycles. b) For ordinary PVDF layers with low lithium ions conductivity and poor mechanical modulus, interfacial fluctuations in which deposits penetrate the PVDF layer occur after cycling. c) PVDF@γ-Fe_2O_3 is conformal and mechanically strong to suppress Li dendrites penetration and stabilize Li metal surface.

Research Article
doi.org/10.1002/batt.202300389
Chemistry Europe
European Chemical Societies Publishing

Here, various properties of the SEI layer can be optimized by adding a small amount of magnetic particle into PVDF (PVDF@γ-Fe_2O_3), as shown in Figure 1(c). A uniformly mixed slurry containing a certain proportion of PVDF and γ-Fe_2O_3 is scraped onto the surface of the current collector. During the drying process, a permanent magnet is added to the surface to magnetize the γ-Fe_2O_3 particles and generate a micro-magnetic field on the electrodes. Under the action of the magneto fluidic effect generated by the magnetic field, the direction of movement of lithium ions is changed, making a spiral motion, causing convection of the electrolyte, thereby improving mass transfer and ion distribution during the charging/discharging process. In addition, the introduction of γ-Fe_2O_3 particles, with a modulus of 203 GPa,[13] further enhances the modulus of the PVDF membrane. Meanwhile, the introduction of γ-Fe_2O_3 can also reduce the crystallinity of PVDF, so that the transport mode of lithium ions changes from the original order domain conduction formed by the folding of the polymer chain to the chain segment movement conduction.[12] Many studies have shown that the phase interface between two species (in this case, metal oxide and polymer) is also a transport channel for lithium ions.[14] Therefore, the introduction of magnetic particles enables the construction of a bifunctional SEI, which not only enhances the mechanical properties of the SEI but also enhances the conduction rate of lithium ions.

To verify the diffusion enhancement by magnetic SEI, comprehensive electrochemical characterizations were conducted to evaluate the kinetics of lithium migration through SEI. Copper (Cu) foils with different coatings were applied for electrochemical impedance spectroscopy (EIS) analysis. The as-obtained EIS profiles are shown in Figure 2(a, b) and Table S1. By constructing equivalent circuits (Figure S1), it was observed that the interfacial impedance of the spontaneously generated SEI layer on the surface of the lithium metal anode was about 85.8 Ω, and that of the SEI film coated with the ordinary PVDF coating was about 48.1 Ω. The X-Ray Diffraction (XRD) and Fourier transform infrared spectroscopy (FTIR) characterization showed that the coating generated on the copper current collector surface was β-phase PVDF (Figure S2), which fulfilled a higher lithium-ion diffusion rate, so the interface impedance

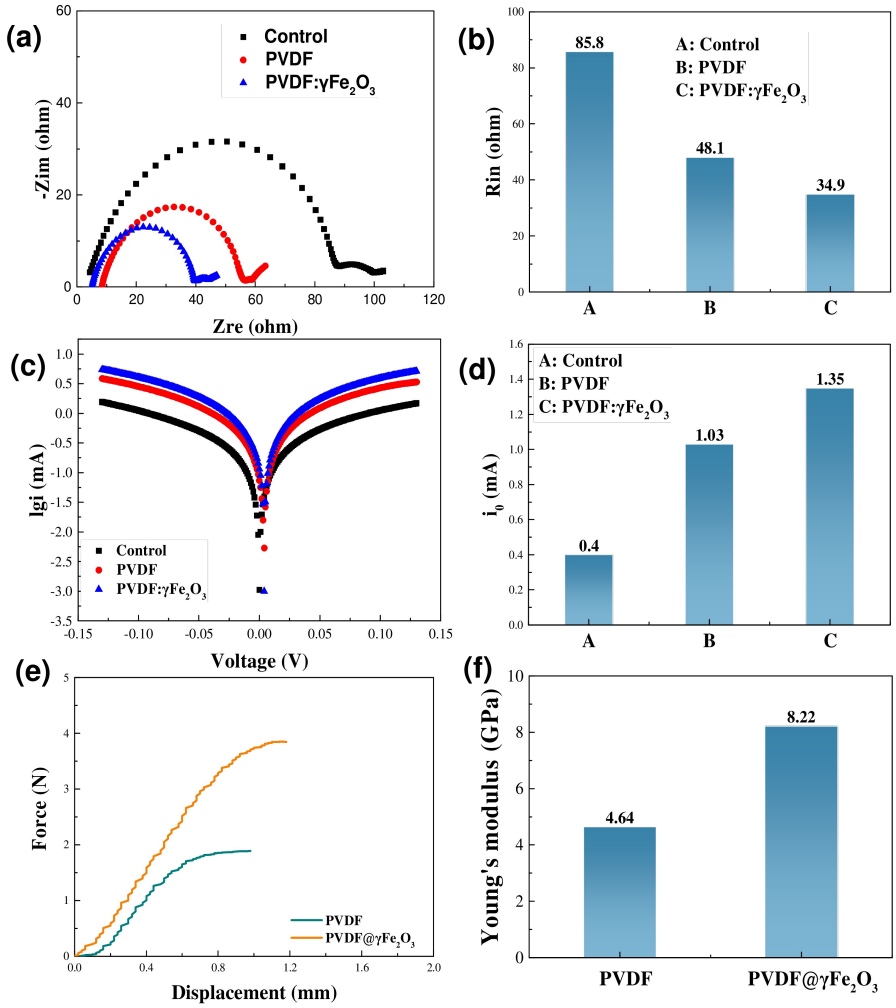

Figure 2. Electrochemical characterizations and mechanical properties of the different coatings. a) Electrochemical impedance spectra (EIS) of different coatings (including control case, ordinary PVDF, and magnetic SEI). b) The corresponding SEI resistance (Rin) calculated from the result a). c) Tafel plots and corresponding d) exchange current of control case, ordinary PVDF, and magnetic SEI. e) The force-distance curve and f) the corresponding fitting Young's modulus value of the ordinary PVDF and magnetic SEI.

was significantly lower than that of the native SEI. While the interfacial impendence of the magnetic SEI film-coated sample was further reduced to 34.9 Ω. To verify the optimization effect of the interfacial micro-magnetic field on the mass transfer of lithium ions, PVDF was further mixed with non-magnetic particles to obtain PVDF-Al_2O_3 coating (40:1). The EIS test showed that the non-magnetic interface impedance was 44.6 Ω (Figure S3), indicating that the magnetic field generated by magnetic particles at the interface can induce faster deposition and stripping of lithium ions. At the same time, the activation energy of Li ions diffusion in SEI was further investigated by temperature-dependent electrochemical impedance spectroscopy (EIS) in the range of 273–308 K. The interface impedance and diffusion activation energy can be correlated by the Arrhenius equation (Figure S4). As shown in Figure S4 and S5, the activation energy for Li-ion diffusion through SEI reduced from 64.0 kJ mol^{-1} in the control case, to 59.4 kJ mol^{-1} in ordinary PVDF, and 55.5 kJ mol^{-1} in magnetic SEI, respectively. At different temperatures, the interfacial ionic conductivity of the electrode coated with magnetic SEI was much higher than that of the control case and the ordinary PVDF electrode (Table S2). The results showed that the introduction of magnetic particles can increase the transmission channels of lithium ions and enhance the movement of ions in the chain segments of the PVDF, thus reducing the interface impedance of the electrode. Furthermore, the Tafel plots of all samples were probed and obtained from the cyclic voltammetry (CV) profiles in Figure S6. The exchange current (j_0) was calculated from the corresponding Tafel plots to reflect charge-transfer kinetics in SEI formed in different electrolytes. As shown in Figure 2(c, d), the control case, ordinary PVDF, magnetic SEI demonstrated increasing exchange current density of 0.40, 1.03, and 1.35 mA cm^{-2}, indicating the faster kinetics of magnetic SEI and thus adequate Li ion beneath the magnetic SEI to achieve uniform Li deposition. Another of the most profound influences magnetic particles bring to the SEI was the enhanced mechanical properties. With rigid magnetic particles incorporated, the SEI exhibited Young's modulus of 8.22 GPa (Figure 2e, f), which far exceeds that of pristine SEI (≈150 MPa)[15] and pristine PVDF layer (4.64 GPa, Figure 2e, f). Such a high modulus endows the magnetic SEI with a strong ability to mechanically block the lithium dendrites, and a modulus of 6 GPa was predicted to be fully qualified for the function of "barrier".[16] Therefore, bifunctional artificial magnetic SEI layers with high ionic conductivity and high mechanical properties were constructed.

To evaluate the effect of the magnetic SEI layer on the deposition behavior of lithium, SEM was employed to evaluate the morphology of deposited lithium, as shown in Figure 3 and Figures S7–S9. The charge/discharge test with Cu foil can directly reflect the influence of different original/artificial SEI on the morphology of lithium deposition and stripping. Thus, detailed observations of the electrode surface morphology after the first lithium deposition and multiple charge-discharge have been finished. When lithium was deposited on bare copper foil at a current density of 0.5 mA cm^{-2} to 1.0 mAh cm^{-2}, the deposition morphology on the surface was mainly irregular dendrite structure, as shown in Figure S8. This may be due to the existence of slip lines and kinks on the surface of Cu foil (Figure S7), and the limited diffusion of lithium ions, resulting in a higher consumption rate of lithium ions at the interface than the supply rate, forming a concentration gradient of lithium ions and inducing the formation of lithium dendrites. Under the same charge-discharge conditions, after the first deposition, the surface of the Cu electrode coated with ordinary PVDF and magnetic SEI coatings still maintained the original morphology (Figure S8b–h). This indicates that both artificial coatings can inhibit the growth of dendrites in a short cycle time. The Energy Dispersive Spectrometer (EDS) mapping showed that the distribution of elements on the electrode surface was very uniform, and the composition of magnetic SEI did not change signally (Figure S10). This indicates that the γ-Fe_2O_3 in artificial magnetic SEI is effectively protected, possibly due to the magnetic particles being fixed in the upper half of the coating during the magnetization process (Figure S11). After lithium plating, cleaning the Cu electrode with solvent found that the lithium deposition layer on the surface of the control electrode very easily fell off from the collector to form "island" lithium. Instead, the lithium metal was firmly held in place on electrodes coated with a magnetic SEI layer (Figure S12). Furthermore, it was attempted to investigate the Li deposition morphology and SEI integrity after long-term cycling (after the Aurbach CE tests at 1 mA cm^{-2}) by SEM. After long-term experiments, the lithium deposition morphology of electrodes not coated with any artificial SEI still maintained a loose porous structure, which is very prone to shed "dead lithium" from the electrode (Figure 3a). This would lead to a continuous decrease in the content of active substances, which reduces the lithium battery capacity. At the same time, the SEI film on the surface of metallic lithium was destroyed, and it was difficult to observe the complete protective layer. The electrode coated with ordinary PVDF coating no longer maintained the original morphology, and a large number of cracks appeared on the surface (Figure 3b), which easily led to the continuous consumption of the electrolyte on the electrode surface. In contrast, the Li deposition morphology induced by the magnetic SEI film was still dense, and most of the entire electrode surface was not severely damaged (Figure 3d), which is very beneficial to the stable cycling of the battery.

At the same time, the influence of the mass ratio of magnetic particles in the SEI layer (m_{PVDF}:$m_{\gamma\text{-}Fe2O3}$ = 100:1; 60:1; 40:1; 20:1; 10:1; 6:1) on lithium deposition morphology and cell performance was further explored. As shown in Figure 3(c-f) and Figure S8, with the increase of magnetic particle content (from 100:1 to 40:1), the integrity of the SEI film gradually improved after long-term cycles. But unexpectedly, when the number of magnetic particles continued to increase (from 40:1 to 6:1), the SEI film was greatly damaged. The morphology law is highly consistent with the change law of Coulombic efficiency with the content of magnetic particles, and the optimal state appeared when m_{PVDF}:$m_{\gamma\text{-}Fe2O3}$ = 40:1 (Figure 3g and Figure S13). The reason for this phenomenon is most likely that when the number of magnetic particles added was too large, it was easy to agglomerate on the electrode surface, resulting in a smaller effective lithium deposition area and slower lithium-ion trans-

Research Article
doi.org/10.1002/batt.202300389
Chemistry Europe
European Chemical Societies Publishing

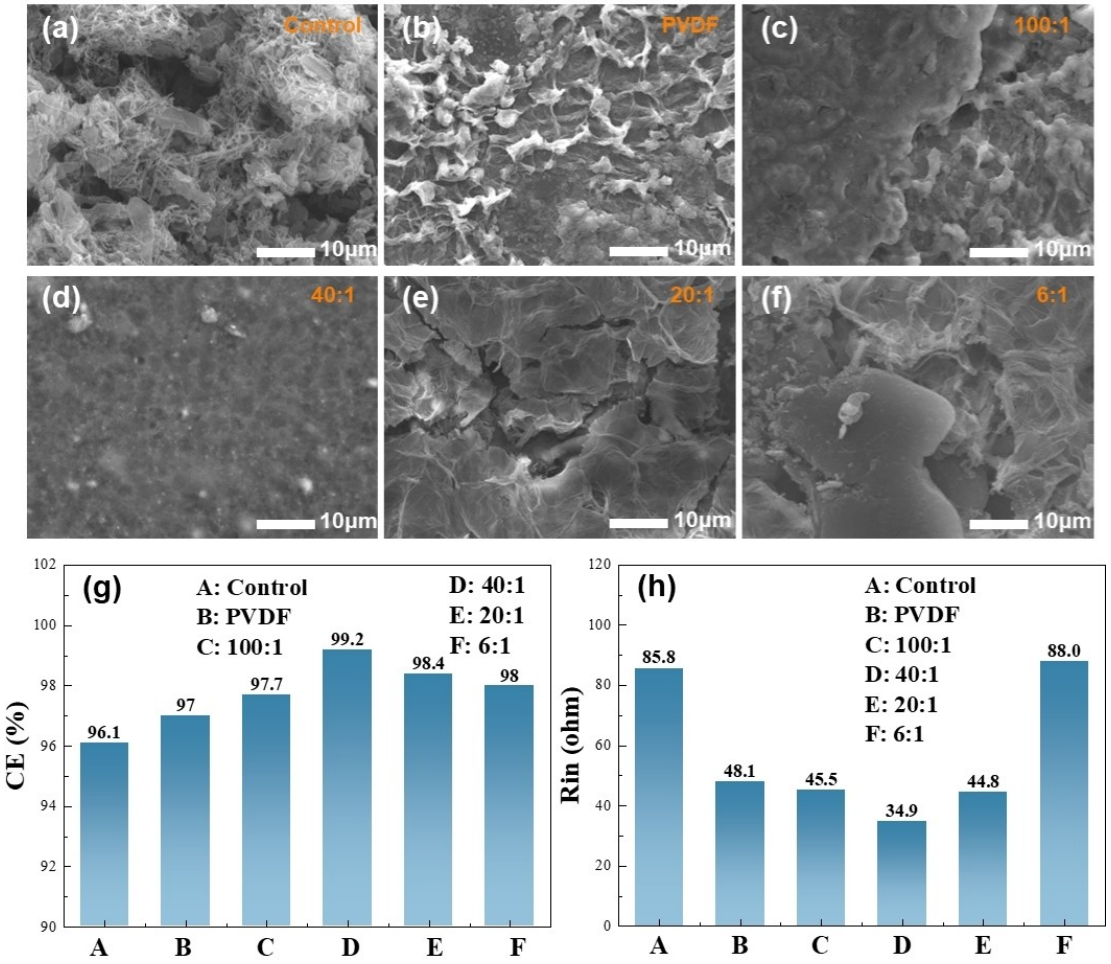

Figure 3. Effect of magnetic particle content on electrode deposition morphology and electrochemical performance in artificial SEI. Morphologies of lithium anode after CE test at a current density of 1.0 mA cm^{-2}: a) bare Cu, b) ordinary PVDF, and c–f) magnetic SEI (PVDF@γ-Fe_2O_3) with various content of magnetic particles from 100:1 to 6:1. g) The variation of Coulombic efficiency with magnetic particle content. h) The variation of interfacial impendence (Rin) with magnetic particle content.

port. It was confirmed by electrochemical impedance spectroscopy analysis, that is, the interfacial resistance first decreased and then increased with increasing magnetic particle content (Figure 3h and Figure S14). In order to better understand and capture the cross-section information of artificial magnetic SEI, scanning electron microscopy (SEM) and focused ion beam scanning electron microscopy (FIB-SEM) were used to observe and compare the cross-section morphology of magnetic SEI and primary SEI. It was found that although the prepared artificial SEI layer had little thickness with the original SEI (Figure S15), the artificial magnetic SEI had higher lithium ions conductivity and lower interface impedance. This indicated that the introduction of artificial magnetic SEI layer has little impact on the overall quality capacity of lithium metal batteries. The above results showed that adding an appropriate number of magnetic particles into PVDF can improve the lithium-ion conductivity and Young's modulus of the artificial SEI film, and inhibit the growth of dendrites from various aspects.

Since the lithium on the Cu@Li electrode came from the electrochemical deposition process, it can be used as the anode to directly and truly reflect the influence of deposition morphology induced by different SEI layers (the control case, the ordinary PVDF and the magnetic SEI) on the cells cycle performance and service life. Therefore, Cu@Li|Li cells were constructed to explore the polarization behavior and stability of lithium anodes, as shown in Figure 4. When the current density was 0.5 mA cm^{-2} (Figure 4a), the unmodified battery holding voltage hysteresis overshoot was less than 200 hours. This is most likely caused by dendrite growth, SEI layer rupture, and continuous electrolyte consumption. When the lithium anode was covered by ordinary PVDF, the cell holding voltage hysteresis exceeded 500 h. It may be due to the fact that ordinary polymer SEI can also play a certain and limited role in inhibiting dendrite growth and propagation. Surprisingly, when the electrode surface was coated with magnetic SEI, the stable cycle time of the Cu@Li|Li cell was greatly improved, exceeding 4000 h, which is longer than the cycle time under the same test conditions reported in most of the current literature (Table S3). The excellent cycling performance was also supported by the overpotential information. After the 50th cycle, the overpotential of control cells (~150 mV) was about 7.5 times that of cells with magnetic SEI (~20 mV) (Figure 4b). When the current

Research Article
doi.org/10.1002/batt.202300389
Chemistry Europe
European Chemical Societies Publishing

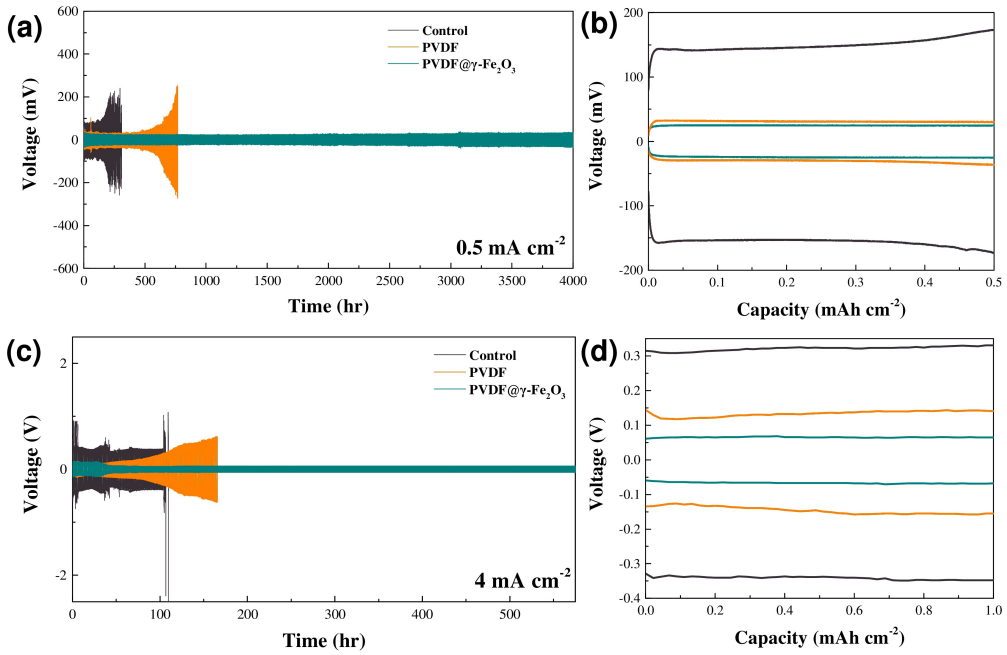

Figure 4. Cycling Stability of Cu@Li|Li Cells. a) Voltage-time curves of Cu@Li|Li coin cells at a current density of 0.5 mA cm^{-2} and b) corresponding voltage profiles of the 50th cycles. c) Voltage-time curves of Cu@Li|Li coin cells at a current density of 4.0 mA cm^{-2} and d) corresponding voltage profiles of the 100th cycles.

density is 4 mA cm^{-2}, as shown in Figure 4(c, d), it was difficult for the control case to carry out a stable charge-discharge long cycle. When the lithium anode was covered by the ordinary PVDF, the cell holding voltage hysteresis was over 100 h. When the electrode surface was coated with the magnetic SEI (PVDF@γ-Fe_2O_3), the stable cycle time of the battery can also exceed 500 h. The above results prove that the magnetic SEI layer can optimize the reaction-diffusion behavior of the interface, induce uniform lithium deposition/stripping, and achieve an efficient and long cycle of symmetric cell.

To confirm the role of magnetic SEI in improving the stability and rate performance of cells, two kinds of cell systems, Li|Cu cell and Li|LFP cell were constructed and cycled with different coatings, as shown in Figure 5. Among them, Li|Cu cells with different coatings were constructed to measure Coulombic efficiency (CE). The average CE of the cell with the magnetic SEI layer exceeded 98% after 110 cycles running at 0.5 mA cm^{-2} to 0.5 mAh cm^{-2}, while the CE of the control cell was reduced to 63% after 60 cycles and the CE of the cell with ordinary SEI was reduced to about 75% after 70 cycles, as shown in Figure 5a. The Aubach CE test method was also employed to measure the Coulombic efficiency of the cells. As shown in Figure 5b, at a current density of 1 mA cm^{-2}, the application of the magnetic SEI (PVDF@γ-Fe_2O_3) resulted in a significant increase in CE (99.2%) compared to the control case (96.1%) and the ordinary PVDF (97.0%). When the current density was increased to 4.0 mA cm^{-2}, the cell with a magnetic SEI layer kept a high CE (98.6%), as shown in Figure S16, indicating the diffusion rate of Li^+ through the magnetic SEI layer is compatible with the high reaction rate. To demonstrate that magnetic fields generated by magnetic particles have an additional positive effect on the deposition/stripping process. The Coulombic efficiency of the battery coated with non-magnetic SEI (PVDF-Al_2O_3) was tested at 1 mAcm^{-2}. It was found that the CE value of the battery coated with magnetic SEI film (99.2%) was much higher than that of the battery coated with non-magnetic SEI (97.7%), as shown in Figure S17. Furthermore, the cycling performance of the Cu@Li|LFP cell was studied. At a discharge rate of 1.0 C, the cell optimized by the magnetic SEI exhibits better cycling performance. As depicted in Figure 5(c, d), in the electrolytic liquid system, the Cu@Li|LFP full cells covered with a magnetic SEI maintained capacity retention of more than 90% after the 400th cycle. Compared with the performance of Cu@Li|LFP cells reported in many literatures, this result has more cycles and higher capacity retention rate (Table S4). In contrast, the capacity of the cell with ordinary PVDF and the control cell dropped rapidly to a retention of 70% after the 250th cycle. Meanwhile, the specific capacity of the cell with the magnetic SEI layer exceeded 140 mAh g^{-1} after the 250th cycle. After long-term cycling, the electrode surface of the optimized battery was also smoother and the SEI maintains good integrity (Figure S18). Therefore, in the full battery, the magnetic artificial SEI can help to achieve an efficient and reversible stable long cycle by inducing more uniform lithium deposition. It is worth noting that the capacities of full batteries covering different SEIs fluctuated periodically with the number of cycles. This may be the oscillation effect of the battery testing system on the same batch of batteries. In addition, Figure 5(e, f) showed the obtained rate capability of the Cu@Li|LFP cells (with various coatings) in the charging rate range from 0.08 to 1.6 C, followed by a recovery at 0.08 C. It was found that the difference in discharge capacities between cells with

Research Article
doi.org/10.1002/batt.202300389
Chemistry Europe
European Chemical Societies Publishing

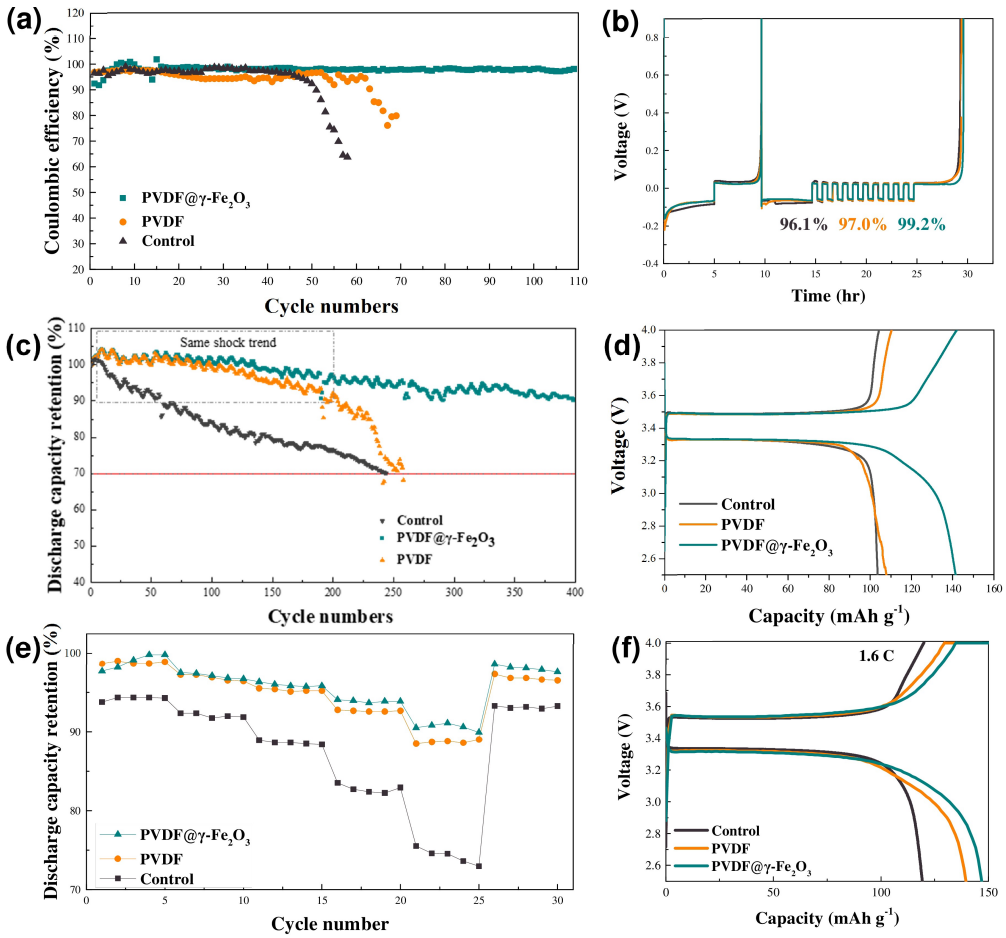

Figure 5. Cycling performance of lithium batteries with various SEI layers. a) Cycling performance and Coulombic efficiency (CE) of Li plating/stripping on Cu foil at 0.5 mA cm^{-2}. b) Aurbach measurement of Li metal CE in Li|Cu half cells at 1.0 mA cm^{-2}. c) Cycling performance of Cu@Li|LFP cell under the charging rate of 1.0 C. d) Corresponding voltage profiles of the 250th cycles. e) The rate capability of a Cu@Li|LFP cell under different charging rates (0.08, 0.24, 0.4, 0.8, 1.6 C). f) The voltage profiles at 1.6 C.

artificial SEI and native SEI was impressive at various charging rates. Whether at low or high rates, batteries coated with artificial SEI layers have a significant increase in capacity compared with control cells. At the high charge/discharge rate of 1.6 C, the specific capacity of cells coated with the magnetic SEI layer was 146 mA g^{-1}, and the capacity retention remained above 90%, while the average capacity retention rate of cells coated with ordinary PVDF layer was about 87%, and the capacity retention rate of cells in the control group was as low as 76%. Hence, coating a layer of magnetic SEI on the electrode surface can not only accelerate the conductivity of lithium ions at the interface so that the ion diffusion process at the interface matches the reaction and the ion distribution is more uniform, but also improve the mechanical properties of SEI, inhibit the formation and growth of dendrites, and achieve uniform lithium deposition/stripping effect.

Conclusions

In summary, we designed a dual-functional artificial magnetic SEI with high ionic conductivity and strong mechanical properties to reach stable and long-term cycling of lithium metal batteries. The magnetic SEI consists of a soft PVDF organic base and rigid γ-Fe_2O_3 inorganic particles. The introduction of magnetic particles optimized the conduction mode of lithium ions in PVDF, from slow "tunnel" transport to fast chain movement. It also made lithium ions more evenly distributed at the electrode interface. At the same time, the rigid γ-Fe_2O_3 improved the overall Young's modulus of the layer and hindered the growth and spread of lithium dendrites. Surprisingly, the stable cycle life of the symmetrical cell coated with the magnetic protection layer was 19 times more than that of the control cell, which is far higher than most data reported in the past. Meanwhile, the Coulombic efficiency (CE) of Li|Cu cells with magnetic SEI was as high as 99.2%. After coating the magnetic SEI, the cell combined with $LiFePO_4$ cathode and the magnetic protective lithium anode has a higher capacity retention rate, which is higher than 90% after 400 cycles at the 1 C rate. The design of the magnetic artificial protective layer not only provides a practical solution for the preparation and improvement of lithium metal anode, but also proposes a new angle of view to develop efficient batteries by matching the diffusion and reaction processes in batteries.

Research Article
doi.org/10.1002/batt.202300389
Chemistry Europe
European Chemical Societies Publishing

Experimental Section

Materials

The lithium metal anodes (ø15.6 mm×0.45 mm width) were supplied by China Energy Lithium Co., Ltd. Lithium iron phosphate ($LiFePO_4$, LFP) cathodes were purchased from Kelude Corporation. The ether-based electrolyte of 1.0 M lithium bis(trifluromethanesulfonyl)imide (LITFSI)-1,3-dioxolane (DOL)/Dimethyl ether (DME) (1:1 by volume) with 1% $LiNO_3$ were purchased from DoDoChem Co., Ltd. Copper (Cu) foils were ordered from Hefei MTI Corporation. Polyvinylidene fluoride (PVDF) materials and carbon black were also purchased from MTI Corporation. Gamma iron trioxide (γ-Fe_2O_3) nanoparticles were ordered from Aladdin Co., Ltd. The dispersion solvent of N-methyl-2-pyrrolidone (NMP) was bought from Sinopharm Chemical Reagent Co., Ltd.

Fabrication of artificial magnetic protective layer

Firstly, PVDF was dispersed in N-methyl-2-pyrrolidone and magnetically stirred for 6 h. After the slurry is clarified, add γ-Fe_2O_3 with different mass ratios (m_{PVDF}: $m_{\gamma\text{-}Fe2O3}$ = 100:1, 60:1, 40:1, 20:1, 10:1, 6:1). Then, the dispersion was manually pre-stirred with the glass rod for 1 h. And a mechanical homogenizer was used to disperse the slurry at 1×10^5 rpm until the slurry was evenly mixed. After that, the dispersion was doctor-bladed on the Cu foils and transferred to a vacuum oven, followed by drying at 65 °C. During the drying process of the Cu foils with the fluid layer, a permanent magnet was placed above it, so that the magnetic flux density on the surface of the copper sheet was not less than 50 mT. The purpose of this process is to magnetize the magnetic particles in the fluid layer. Prior to use, the film was pouched into pieces with a diameter of 16 mm or 18 mm.

Electrochemical measurement

CR2032 coin cells were used in all experiments. Double layers of Monolayer polypropylene were used as the separator, and each cell was filled with 60 μL 1.0 M LiTFSI DOL/DME-1 wt% $LiNO_3$ electrolyte. Bare Cu foils, Cu foils covered with PVDF (Cu@PVDF), and Cu foils covered with magnetic SEI (Cu@PVDF-γ-Fe_2O_3) were used to assemble various types of cells for performance comparison, and the operation was carried out in an argon-filled glove box with H_2O and O_2 content below 0.1 ppm.

Electrochemical measurements of Li|Cu cells

The Li|Cu cells were charged and discharged in constant current mode on the Microcurrent battery test equipment (Wuhan LAND Electronics Co., Ltd) for the morphology observation after lithium deposition, and Coulombic efficiency (CE) test. Two methods including the conventional CE test and the Aurbach CE test were applied to test the CE.[17]

Electrochemical measurements of Cu@Li|Li cells

Cu@Li|Li cells were used for the examination of the electrochemical cycling performance and comprehensive electrochemical characterization, assembled using a Cu foil and a Li foil as electrodes. The Cu foils (including bare Cu, Cu foils with PVDF, and Cu foils with magnetic SEI) were punched into 18 mm disks as the working electrode, and the diameter of the counter Li electrode was 15.6 mm. For comprehensive electrochemical characterization (EIS and CV), Li with a capacity of 0.5 mAh cm^{-2} or 1.0 mAh cm^{-2} was pre-deposited on Cu sheets at a current density of 0.5 mA cm^{-2} to form Cu@Li electrodes. For the cyclic performance test of symmetrical cells, the following pretreatment was required to form a certain lithium coating: Firstly, the lithium was deposited on the Cu foil to 10 mAh cm^{-2}, then the lithium was stripped to 0.9 V, and then the copper foil was plated with 10 mAh cm^{-2} lithium in the shape of Cu @Li electrode. The charge-discharge cycle test for symmetric batteries was performed at current densities of 0.5 mA cm^{-2} or 4.0 mA cm^{-2}.

Electrochemical impedance spectroscopy (EIS) measurements and cyclic voltammetry (CV) tests were performed on the CHI660E electrochemical workstation provided by Shanghai Chenhua Corporation. EIS tests range from 0.1–10^5 Hz in frequency and 273–308 K in temperature. The test results of EIS were analyzed by Zview software, and the interface diffusion parameters were calculated by the impedance values under the test condition of temperature variation. The CV scan rate was 0.5 mV s^{-1} and the scan voltage window was from −0.15 to 0.15 V, respectively.

Cu@Li|LFP cells assembly and electrochemical measurements

Cu@Li|LFP cells were used to test the rate capability and cycling performance. Polyvinylidene fluoride (PVDF, 10 wt.%) was added to N-methyl-2-pyrrolidone (NMP, Sinopharm Chemical Reagent Co., Ltd) and magnetically stirred for 6 h, and then active substance ($LiFePO_4$, 80 wt.%) and conductive carbon black (10 wt.%) were added to the viscous solution and stirred for 24 h. Scraped and applied the above mixture onto Al foil and vacuum dried at 80 °C for one night. After cutting, the positive electrode sheet was obtained. The Cu@Li|LFP cells were assembled and tested as follows: (1) deposited lithium at 0.3 mA cm^{-2} on Cu foils (including bare Cu, Cu foils with PVDF, and Cu foils with magnetic SEI) as Cu@Li electrode; (2) Assembled Cu@Li electrode and LFP cathode into full cells; (4) Charged-discharged tests at different rates.

Characterizations

The morphology of the deposited Li was determined by an extremely high-resolution scanning electron microscope (SEM, JSM 7401F, JEOL). The operation voltage of the SEM was 10.0 kV or 15.0 kV. The Cu foils after Lithium deposition of 1 mAh cm^{-2} at a current density of 0.5 mA cm^{-2} were used for morphology characterization. The morphology of lithium deposition/stripping and the integrity of SEI were explored by SEM after long-term cycles (after the Aurbach CE tests at 1 mA cm^{-2}). The morphology of the pristine SEI was determined by focused ion beam-scanning electron microscope (FIB-SEM, JIB-4700F, JEOL). A rough cross-sectional milling (30 kV, 1000 pA) was done on the anode by the FIB (Ga beam). In order to remove residual lithium salts on electrode surfaces after cycling, all samples were rinsed with solvent three times before being used for morphology observation and placed overnight on an electric heating plate in the glove compartment. The test samples were transferred to the characterization equipment in a closed container to ensure that the samples were not contaminated by air to the maximum extent. The crystalline phase of the PVDF/PVDF@γ-Fe_2O_3 coatings was confirmed by Fourier transformed infrared spectroscopy (FTIR) (NICOLET iS 50) and X-ray diffraction (XRD) (Smartlab (9)). Samples were obtained by peeling the artificial coatings off the Cu substrate.

Supporting Information

Supporting Information is available from the Wiley Online Library or from the author. The authors have cited additional references within the Supporting Information (Ref. [18]).

Acknowledgements

This work was supported by the National Natural Science Foundation of China (91934302, 21978298, U1862117), the Innovation Academy for Green Manufacture, Chinese Academy of Sciences, and the project from the State Key Laboratory of Multiphase Complex Systems (MPCS-2021-A-05).

Conflict of Interests

The authors declare no conflict of interest.

Data Availability Statement

The data that support the findings of this study are available from the corresponding author upon reasonable request.

Keywords: lithium metal anode · solid electrolyte interphase (SEI) · magnetic SEI · diffusion enhancement

[1] a) D. Lin, Y. Liu, Y. Cui, *Nat. Nanotechnol.* **2017**, *12*, 194; b) X. Zhang, Y. Yang, Z. Zhou, *Chem. Soc. Rev.* **2020**, *49*, 3040; c) Y. X. Zhan, P. Shi, R. Zhang, X. Q. Zhang, X. Shen, C. B. Jin, B. Q. Li, J. Q. Huang, *Adv. Energy Mater.* **2021**, *11*, 2101654.
[2] C. Jin, T. Liu, O. Sheng, M. Li, T. Liu, Y. Yuan, J. Nai, Z. Ju, W. Zhang, Y. Liu, Y. Wang, Z. Lin, J. Lu, X. Tao, *Nat. Energy* **2021**, *6*, 378.
[3] a) A. Hu, W. Chen, X. Du, Y. Hu, T. Lei, H. Wang, L. Xue, Y. Li, H. Sun, Y. Yan, J. Long, C. Shu, J. Zhu, B. Li, X. Wang, J. Xiong, *Energy Environ. Sci.* **2021**, *14*, 4115; b) Y. X. Zhan, P. Shi, X. X. Ma, C. B. Jin, Q. K. Zhang, S. J. Yang, B. Q. Li, X. Q. Zhang, J. Q. Huang, *Adv. Energy Mater.* **2021**, *12*, 2103291.
[4] a) X. B. Cheng, R. Zhang, C. Z. Zhao, Q. Zhang, *Chem. Rev.* **2017**, *117*, 10403; b) J. Lu, Z. Chen, F. Pan, Y. Cui, K. Amine, *Electrochem. Energy R.* **2018**, *1*, 35.
[5] a) Z. Wang, F. Qi, L. Yin, Y. Shi, C. Sun, B. An, H. M. Cheng, F. Li, *Adv. Energy Mater.* **2020**, *10*, 1903843; b) X. Q. Zhang, X. Chen, X. B. Cheng, B. Q. Li, X. Shen, C. Yan, J. Q. Huang, Q. Zhang, *Angew Chem.-Int. Ed.* **2018**, *57*, 5301.
[6] S. Gao, F. Sun, N. Liu, H. Yang, P.-F. Cao, *Mater. Today* **2020**, *40*, 140.
[7] a) Y. Chen, Y. Chen, R. Wang, X. Lv, Y. Han, *Chem. Eng. J.* **2022**, *446*, 137435; b) J. Meng, F. Chu, J. Hu, C. Li, *Adv. Funct. Mater.* **2019**, *29*, 1902220.
[8] a) J. Ming, Z. Cao, W. Wahyudi, M. Li, P. Kumar, Y. Wu, J.-Y. Hwang, M. N. Hedhili, L. Cavallo, Y.-K. Sun, L.-J. Li, *ACS Energy Lett.* **2018**, *3*, 335; b) S. Kim, T. K. Lee, S. K. Kwak, N.-S. Choi, *ACS Energy Lett.* **2022**, *7*, 67.
[9] a) Y. Yamada, K. Furukawa, K. Sodeyama, K. Kikuchi, M. Yaegashi, Y. Tateyama, A. Yamada, *J. Am. Chem. Soc.* **2014**, *136*, 5039; b) Y. Yamada, J. Wang, S. Ko, E. Watanabe, A. Yamada, *Nat. Energy* **2019**, *4*, 269.
[10] a) C.-C. Su, M. He, R. Amine, Z. Chen, R. Sahore, N. Dietz Rago, K. Amine, *Energy Storage Mater.* **2019**, *17*, 284; b) T. Li, X.-Q. Zhang, P. Shi, Q. Zhang, *Joule* **2019**, *3*, 2647.
[11] a) W. Liu, P. Liu, D. Mitlin, *Adv. Energy Mater.* **2020**, *10*, 2002297; b) Y. Gao, Z. Yan, J. L. Gray, X. He, D. Wang, T. Chen, Q. Huang, Y. C. Li, H. Wang, S. H. Kim, T. E. Mallouk, D. Wang, *Nat. Mater.* **2019**, *18*, 384; c) R. M. Gao, H. Yang, C. Y. Wang, H. Ye, F. F. Cao, Z. P. Guo, *Angew Chem.-Int. Ed.* **2021**, *60*, 25508.
[12] R. Xu, X.-Q. Zhang, X.-B. Cheng, H.-J. Peng, C.-Z. Zhao, C. Yan, J.-Q. Huang, *Adv. Funct. Mater.* **2018**, *28*, 1705838.
[13] J. Z. Jiang, O. J. Staun, L. Gerward, S. Morup, Europhys. Lett. 1998, 44, 620.
[14] a) X. Wen, K. Liang, L. Tian, K. Shi, J. Zheng, *Electrochim. Acta* **2018**, *260*, 549; b) A. Ramasubramanian, V. Yurkiv, T. Foroozan, M. Ragone, R. Shahbazian-Yassar, F. Mashayek, *J. Phys. Chem. C* **2019**, *123*, 10237.
[15] X. R. Liu, X. Deng, R. R. Liu, H. J. Yan, Y. G. Guo, D. Wang, L. J. Wan, *ACS Appl. Mater. Interfaces* **2014**, *6*, 20317.
[16] C. Monroe, J. Newman, *J. Electrochem. Soc.* **2005**, *152*, A396.
[17] a) Y. Chen, H. Huang, L. Liu, Y. Chen, Y. Han, *Adv. Energy Mater.* **2021**, *11*, 2101774; b) B. D. Adams, J. Zheng, X. Ren, W. Xu, J. G. Zhang, *Adv. Energy Mater.* **2017**, *8*, 1702097.
[18] a) B. Han, Y. Zou, Z. Zhang, X. Yang, X. Shi, H. Meng, H. Wang, K. Xu, Y. Deng, M. Gu, *Nat. Commun.* **2021**, *12*, 3066; b) R. Pathak, K. Chen, A. Gurung, K. M. Reza, B. Bahrami, J. Pokharel, A. Baniya, W. He, F. Wu, Y. Zhou, K. Xu, Q. Qiao, *Nat. Commun.* **2020**, *11*, 93; c) W. Cao, J. Lu, K. Zhou, G. Sun, J. Zheng, Z. Geng, H. Li, *Nano Energy* **2022**, *95*, 106983; d) Q. Wang, J. Yang, X. Huang, Z. Zhai, J. Tang, J. You, C. Shi, W. Li, P. Dai, W. Zheng, L. Huang, S. Sun, *Adv. Energy Mater.* **2022**, *12*, 2103972; e) N. W. Li, Y. Shi, Y. X. Yin, X. X. Zeng, J. Y. Li, C. J. Li, L. J. Wan, R. Wen, Y. G. Guo, *Angew Chem.-Int. Ed.* **2018**, *130*, 1521; f) K. Chen, R. Pathak, A. Gurung, E. A. Adhamash, B. Bahrami, Q. He, H. Qiao, A. L. Smirnova, J. J. Wu, Q. Qiao, *Energy Storage Mater.* **2019**, *18*, 389; g) J. Holoubek, Q. Yan, H. Liu, E. J. Hopkins, Z. Wu, S. Yu, J. Luo, T. A. Pascal, Z. Chen, P. Liu, *ACS Energy Lett.* **2022**, *7*, 675; h) C. Z. Zhao, Q. Zhao, X. Liu, J. Zheng, S. Stalin, Q. Zhang, L. A. Archer, *Adv. Mater.* **2020**, *32*, 1905629; i) H. Zhang, J. Luo, M. Qi, S. Lin, Q. Dong, H. Li, N. Dulock, C. Povinelli, N. Wong, W. Fan, *Angew Chem.-Int. Ed.* **2021**, *60*, 19183; j) W. Lu, L. Sun, Y. Zhao, T. Wu, L. Cong, J. Liu, Y. Liu, H. Xie, *Energy Storage Mater.* **2021**, *34*, 241; k) R. Xu, Y. Xiao, R. Zhang, X. B. Cheng, C. Z. Zhao, X. Q. Zhang, C. Yan, Q. Zhang, J. Q. Huang, *Adv. Mater.* **2019**, *31*, 1808392; l) P. Li, X. Dong, C. Li, J. Liu, Y. Liu, W. Feng, C. Wang, Y. Wang, Y. Xia, *Angew Chem.-Int. Ed.* **2019**, *131*, 2115; m) C. Chen, J. Zhang, B. Hu, Q. Liang, X. Xiong, *Nat. Commun.* **2023**, *14*, 4018; n) K. Huang, S. Song, Z. Xue, X. Niu, X. Peng, Y. Xiang, *Energy Storage Mater.* **2023**, *55*, 301; o) Y. Nie, X. Dai, J. Wang, Z. Qian, Z. Wang, H. Guo, G. Yan, D. Jiang, R. Wang, *J. Energy Chem.* **2022**, *75*, 285.

Manuscript received: September 7, 2023
Revised manuscript received: November 1, 2023
Version of record online: December 6, 2023